Dispersion of silica-encapsulated DNA magnetic particles in a homogeneous sand tank

Chakraborty, Swagatam; Elhaj, Rayan; Foppen, Jan Willem; Schijven, Jack F.

DOI
10.1016/j.jconhyd.2024.104410

Publication date
2024

Document Version
Final published version

Published in
Journal of Contaminant Hydrology

Journal of Contaminant Hydrology 266 (2024) 104410

Contents lists available at ScienceDirect

Journal of Contaminant Hydrology

journal homepage: www.elsevier.com/locate/jconhyd

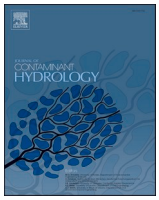

Dispersion of silica-encapsulated DNA magnetic particles in a homogeneous sand tank☆

Swagatam Chakraborty [a,*], Rayan Elhaj [b], Jan Willem Foppen [b,d], Jack F. Schijven [a,c]

[a] Environmental Hydrogeology Group, Department of Earth Sciences, Utrecht University, Princetonlaan 8a, 3584 CB Utrecht, the Netherlands
[b] Department of Water Sciences and Engineering, IHE-Delft, Institution for Water Education, Westvest 7, 2611 AX Delft, the Netherlands
[c] Department of Statistics, Informatics and Modelling, National Institute of Public Health and the Environment, P.O. Box 1, 3720 BA Bilthoven, the Netherlands
[d] Water Resource Section, Department of Civil Engineering and Geoscience, Delft University of Technology, Delft, the Netherlands

ARTICLE INFO

Keywords:
Longitudinal dispersivity
Transverse dispersivity
Colloids
Sand tank
DNA particles

ABSTRACT

In this study, we focused on the 3D dispersion of colloids. To our knowledge, we were the first to do so. Thereto, we injected silica encapsulated DNA tagged superparamagnetic particles (SiDNAmag) in a homogeneous coarse grain sand tank. At four downstream locations, SiDNAmag concentrations were determined as a function of time. Longitudinal and transverse dispersivity values and associated uncertainties of SiDNAmag were determined using Monte Carlo modelling approach. The parameter associated uncertainties of hydraulic conductivity as well as of the effective porosity estimated from SiDNAmag breakthrough curves were statistically similar to those estimated from salt tracer breakthrough curves. Further, the SiDNAmag dispersivity uncertainty ranges were then statistically compared with the salt tracer (NaCl, and fluorescein) dispersivities. Our results indicated that time to rise, time of peak concentration and shape of the breakthrough curves of SiDNAmag were similar to those of the salt tracer breakthrough curves. Despite the size difference between the salt tracer molecules and SiDNAmag, size exclusion did not occur, probably due to the large pore throat diameter to SiDNAmag diameter ratio. The median longitudinal dispersivity (α_L) of salt tracer and SiDNAmag were 4.9 and 5.8 $\times$ 10^{-4} m, respectively. The median ratio of horizontal and vertical transverse dispersivities to α_L, (α_{TH} /α_L and α_{TV} /α_L, respectively), for salt tracer and SiDNAmag ranged between 0.52 and 0.56. Through the statistical tests, we concluded that the longitudinal and traverse dispersivities of SiDNAmag were not statistically significantly different from salt tracer in 3 dimensions and could be used to characterize the dispersive properties of the medium we used. Our work contributes to a better understanding of 3D dispersion of SiDNAmag in saturated porous media.

1. Introduction

Estimation of longitudinal (α_L), horizontal transverse (α_{TH}), and vertical transverse dispersivities (α_{TV}) of colloids in sand is important to predict transport of colloids through sand (Chrysikopoulos and Katzourakis, 2015), and colloid associated contaminant transport (McCarthy, 2018; Won et al., 2019).

In understanding colloid transport through saturated sand, a usual approach is to consider the α_L of salt tracer and colloids to be identical (Schijven et al., 2013; Tosco et al., 2012; Wang et al., 2012). Where few saturated sand column studies have observed similar arrival and time to peak for colloids as compared to conservative tracers (Solovitch et al., 2010; Tosco et al., 2012; Wang et al., 2012), others have reported otherwise. In a number of saturated sand column studies, with a collector grain to colloid diameter ratio ranging between 100 and 110,000 [−] at average linear velocities ranging between 0.1 and 1.95 cm/min (Table 1), an earlier arrival, earlier time to peak and higher longitudinal dispersivity of colloids as compared to salt tracers, were attributed to velocity enhancement due to size exclusion of colloids and effective porosity reduction (Bennacer et al., 2013; Chrysikopoulos and Katzourakis, 2015; Chrysikopoulos and Syngouna, 2014; Grolimund et al., 1998; Higgo et al., 1993; Keller et al., 2004; Mikutis et al., 2018). A positive correlation of colloid size and longitudinal dispersivity was reported by Katzourakis and Chrysikopoulos (2021), and was attributed

☆ *Re*-submission of manuscript (Reference number: CONHYD-D-24-00223).

* Corresponding author.
E-mail address: s.chakraborty@uu.nl (S. Chakraborty).

https://doi.org/10.1016/j.jconhyd.2024.104410
Received 27 May 2024; Received in revised form 17 July 2024; Accepted 22 July 2024
Available online 23 July 2024

to the exclusion of larger colloids from the lower velocity regions of parabolic velocity profile of the pore throats. In micromodels, Sirivithayapakorn and Keller (2003), and James and Chrysikopoulos (2003), reported a reduction in the longitudinal dispersion coefficient and dispersivity with increasing colloid size as compared to conservative tracers. The dispersivity reduction with increasing colloid size was due to smaller colloids and the colloids migrating near the collector grain walls tended to remain near the collector grain wall without migrating to the higher velocity streamlines due to negligible diffusion, therefore, following a more tortuous path (James and Chrysikopoulos, 2003).

In addition to size exclusion and velocity enhancement, colloid retention by straining or attachment onto the collector grains could affect the longitudinal dispersivity of colloids (Vasiliadou and Chrysikopoulos, 2011; Syngouna and Chrysikopoulos, 2011) and overshadow the effect of size exclusion and velocity enhancement by colloid retardation (Grolimund et al., 1998; Keller et al., 2004; Pang et al., 2021). Attachment and remobilization of colloids resulted in an increase in the longitudinal dispersivity (de Vries et al., 2022). The minimum pore throat to colloid diameter ratio was <1.5 for size exclusion to occur (Sirivithayapakorn and Keller, 2003). In a pore network model, Meng and Yang (2019) reported that for smaller diameter particles (100 nm particle diameter as compared to 500 nm particle diameter, used by Meng and Yang (2019)), the effect of size exclusion was negligible and did not affect the longitudinal dispersivity estimation. The contrasting outcomes suggested that dispersion was not only dependent on the porous medium properties but also on the physical properties of colloids (e.g. size) and interaction with the collector grains. Because there were no trends identified between colloid dispersion behaviour and experimental physico-chemical conditions, such as, collector grain diameter, colloid diameter, average flow velocity, and pore throat to colloid diameter ratio (Table 1), a colloid (SiDNAmag) and collector grain size specific estimation of α_L is required.

Horizontal transverse (α_{TH}) and vertical transverse (α_{TV}) dispersivities, in addition to α_L, are also important parameters reflecting the mass transfer through the porous medium and overall concentration distribution of a plume (Bijeljic and Blunt, 2007). α_{TV} and α_{TH} are prevalently considered to be an order of magnitude lower than α_L, which may not be true under all flow and solute transport conditions and therefore, should be determined as an independent parameter (Zech et al., 2019). The consideration of α_{TV} and α_{TH} being 1 order or magnitude lower than α_L, was valid only for advection dominated transport (Bijeljic and Blunt, 2007). The knowledge gap that still remained unaddressed is the estimation of α_{TV} and α_{TH} as independent parameters, specifically for colloid transport, in a 3D system.

In order to address this knowledge gap, our objective was to estimate the α_L, α_{TV}/α_L, and α_{TH}/α_L, of colloid, in the form of SiDNAmag, in a 3D, saturated, homogeneous and unconsolidated sand medium and evaluate the associated uncertainties of α_L, α_{TV}/α_L, and α_{TH}/α_L, and compare with the conservative salt tracer. Since our sand to SiDNAmag diameter is at least 1–2 order of magnitude larger than threshold of displaying size exclusion or pore clogging (Sirivithayapakorn and Keller, 2003), and small sized colloids migrate similar to conservative salt tracer (Wang et al., 2013), we hypothesize that under our experimental conditions, α_L, α_{TV}/α_L, and α_{TH}/α_L values and associated uncertainties estimated from SiDNAmag transport would not be statistically significantly different to that of conservative tracers (null hypothesis). In order to attain the objective, we injected two uniquely sequenced SiDNAmags at two injection wells in a homogeneously packed, saturated, coarse grain sand tank. At four downstream locations, we determined the SiDNAmag concentrations as a function of time (breakthrough curves). We further estimated the longitudinal and transverse dispersivities and associated uncertainties by fitting SiDNAmag breakthrough curves through 3D advective-dispersive equation combined with first order kinetic attachment-detachment model (based on least root mean square error) using a Monte Carlo simulation approach.

DNA particles, either naked or encapsulated in polylactic acid, alginate, or silica, had been previously used for investigating subsurface flow properties, contaminant transport, and aquifer characterization in last two decades (Chakraborty et al., 2022; Foppen, 2023; Mikutis et al., 2018; Pang et al., 2020; Zhang et al., 2021). Unlike the salt or dye tracers, uniqueness in the DNA sequences imparts the advantage of DNA particles in concurrent injection experiments without background concentration interference (Chakraborty et al., 2023; Pang et al., 2020). The encapsulation provides stability to the DNA molecules against physico – chemical stressors such as pH, radiation, or enzymatic activities (Pang et al., 2020; Sharma et al., 2012). The additional advantages of DNA particles were high specificity of detection, and low detection limit in polymerase chain reaction (Dahlke et al., 2015; Foppen et al., 2011).

2. Materials and methods

2.1. SiDNAmag and injection suspension preparation

SiDNAmags are spherical colloidal particles with an iron oxide core and silica covering, impregnated with double stranded DNA (dsDNA) molecules (Sharma et al., 2021). The advantage of dsDNA is the low detection limit, high specificity in quantitative polymerase chain (qPCR), no background concentration interference and are unique in

Table 1
Literature overview of experimental conditions and effect on longitudinal dispersivity, size exclusion and velocity of colloids.

Colloids	Study type	d_c (nm)	d_a (μm)	$\sim d_p/d_c$*	$\sim d_t/d_c$*	V_{cons} (cm/min)	Effect on colloid transport		Reference
							α_L (cm)	Size exclusion and velocity	
Silica DNA	Column	159	200–630	918–2890	424–1600	0.75	Increased	Enhanced	Mikutis et al., (2018)
Silica Colloid	Field	107	600	4000	2200	–	–	Similar peak time	Ryan et al., (1999)
Silica colloid	Column	30	0.5–1000	12–24,000	7–13,000	0.17	–	Enhanced	Higgo et al., (1993)
Polystyrene beads	Column	50, 3000	350	5000, 150	2800, 50	0.1, 1	Decreased	Enhanced	Keller et al., (2004)
Polystyrene microspheres	Column	30–5500	2000	50,000–265	27,000–148	0.5–2	Increased with increasing size	Enhanced	Chrysikopoulos and Katzourakis, (2015)
Kaolinite, *Pseudomonas putida*	Column	Kaolinite <2000, *P. putida* = 2400(900)	2000	Kaolinite = 600, *P. putida* = 700	Kaolinite = 340, *P. putida* = 400	0.98–1.95	Increased	Kaolinite retarded, *P. putida* enhanced	Vasiliadou and Chrysikopoulos, (2011)
E. coli	Column	2000 (600)	425–600	155–220	90–120	0.72	Decreased	No enhancement/ retardation	Syngouna and Chrysikopoulos, (2012)

* approximated from $d_p = 0.73d_a$ and $dt = 0.56d_p$ (correlation applicable to simple cubic packing) (Ren and Santamarina, 2018).

nucleotide sequences providing the advantage of multipoint groundwater flow tracing (Mikutis et al., 2018; Pang et al., 2020). The superparamagnetic property of the iron oxide core imparts the advantage of rapid magnetic separation, therefore, there are no sample volume and up-concentration limitations (Sharma et al., 2021).

At first, we diluted 50 µl of stock suspensions of 0.75 mg/ml (~10^{10} particles/ml) of two uniquely sequenced SiDNAmags ($SiDNAmag_1$ and $SiDNAmag_2$) (Particle Engineering Research Centre, NTNU, Norway) to 5 ml (~10^8 particles/ml) of demineralized water. We treated the 5 ml SiDNAmag suspensions with 1 µl of bleach to remove any free DNA. After dividing the 5 ml suspensions into 1 ml aliquots, we washed the SiDNAmags with demineralized water twice by magnetic separation of the SiDNAmags to remove any traces of bleach. We further prepared the injection suspensions by diluting the 5 ml SiDNAmag suspension into 495 ml (~10^6 particles/ml) of tap water (EC 550 µS/cm; pH 7.0; hardness 145.36 mg/l). The diameter of $SiDNAmag_1$ and $SiDNAmag_2$ were 206.4 ± 85.6 nm and 183.9 ± 58.1 nm with a unimodal size distribution and zeta (ζ) potentials of -11 mV and -14 mV in demineralized water, respectively. We measured the hydrodynamic diameter (D_{hyd}) and the electrophoretic mobility of the SiDNAmags (at a concentration of ~10^7 particles/ml) in tap water using Smoluchowski's equation (Malvern Panalytical Zetasizer Nano-Zs ZEN 3600, the Netherlands). The D_{hyd} were measured using 173° dynamic light backscattering.

2.2. Sand tank experiments, and sample analysis

We wet packed a 1.3 m long (1.3 m × 0.7 m × 0.4 m) PVC tank with coarse grain quartz sand (500–700 µm) to represent an unconsolidated, homogeneous aquifer system (Fig. 1). The tank dimension was determined through pre-modelling exercise using flow and solute transport module (MT3D) considering suitable transport length, effect of injection volume of flow, and interaction of injection water with tank boundaries. We ensured the homogeneity of the tank by settling the sand through repetitive saturation and desaturation with tap water. Prior to the experiments, we conducted several small scale (10–20 cm) salt transport experiments to validate the homogeneity of the system. The ζ potential of the sand was measured by grinding the sand and suspending the sand dust in tap water at a concentration of 0.01 g/ml. The sand grain size

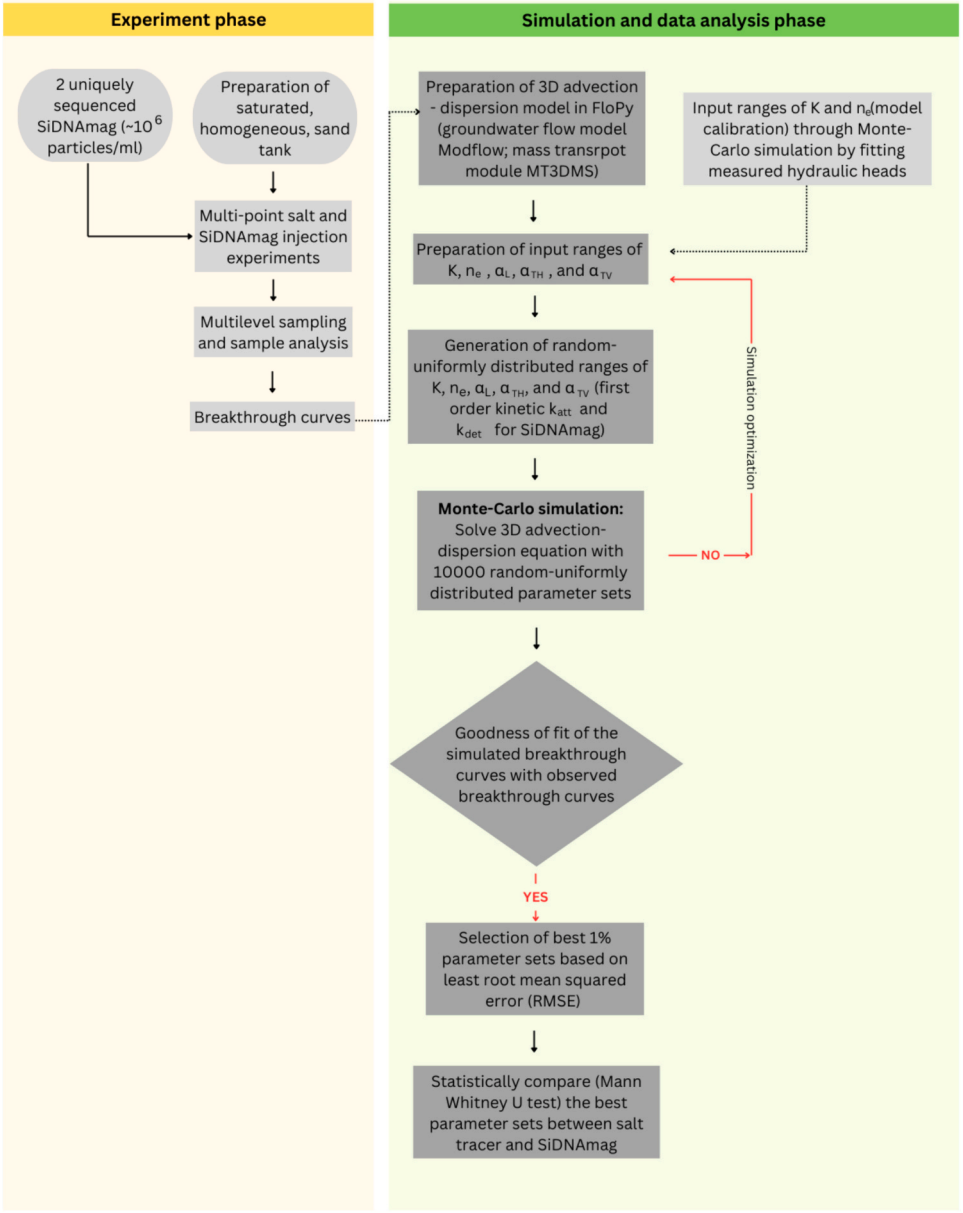

Fig. 1. Laboratory and simulation methodology flowchart.

distribution was measured by dry sieve analysis (Fritsch vibrating sieve, Dijkstra vereenigde, the Netherlands). The d_{60}, d_{50} and d_{10} of the sand were 665, 630, and 370 μm (coefficient on uniformity = $d_{60}/d_{10} = 1.8$), respectively. The bulk density of the sand was 1623 kg/m^3. We estimated the pore diameter (d_p) and pore throat diameter (d_t) from sand grain characteristics using (Ren and Santamarina, 2018)

$$d_p = 8\frac{\sqrt[\gamma]{\frac{K}{K_0}}\,\rho_w G_s D_{50}}{3(C_u+7)\rho_m} \quad (1a)$$

$$d_t = 0.56 d_p \quad (1b)$$

Where γ is the sensitivity of hydraulic conductivity to void ratio. We considered a value of $\gamma = 3$, as suggested by Ren and Santamarina (2018) for coarse gain sand. K is the hydraulic conductivity (m/min), K_0 is the reference hydraulic conductivity at reference void ratio ($e_0 = 1$), ρ_w is the density of sand (g/m^3), G_s is the specific gravity of the sand, D_{50} is the media grain diameter (m), Cu is the coefficient of uniformity and ρ_m is the mass density of the sand (g/m^3) (refer to Ren and Santamarina (2018) for more details). The estimated mean pore diameter to SiDNAmag diameter ratio was $\sim 1.19 \times 10^3 \pm 5.34 \times 10$ (Auset and Keller, 2004). The median pore throat diameter to SiDNAmag diameter ratio was $\sim 6.69 \times 10^2 \pm 2.99 \times 10$ (Auset and Keller, 2004).

We installed two injection wells and one multilevel sampling well at a longitudinal distance of 0.3 m (Inj_1), 0.6 m (Inj_2), and 1.1 m (W_1, W_2, W_3) from the inflow chamber, respectively on single flowline. The screens of the injection wells were installed at a depth of 13–16 cm from the bottom of the tank. The screens of the multilevel sampling well were installed at depths of 7–10 cm, 13–16 cm, and 19–22 cm from the bottom of the tank. Another sampling well (W_4) was placed 3 cm – 4 cm away from the multilevel sampling well, transverse horizontally perpendicular to the flow line (Fig. 2).

At first, we conditioned the sand with flowing tap water for 14–15 h. During the experiments, tap water was constantly pumped (Masterflex 7528–30, Vernon Hills, USA) into the inflow chamber at a rate of 511 ± 7.1 ml/min. Inflow (511 ± 7.1 ml/min) and outflow (505 ± 7.3 ml/min) rates (water balance discrepancy <5%) were monitored gravimetrically (SBSPF100A1, Steinberg Systems, Germany) in order to maintain a steady inflow. We monitored the hydraulic heads manually at 8 different locations inside the sand tank and by water level data loggers at the inflow (~0.36 ± 0.002 m) and outflow (~0.31 ± 0.001 m) chambers (Fig. 2) (TD-Diver, Van Essen Instruments B. V., the Netherlands). Further, we injected (Dirac pulse) 100 ml of 0.017 g/l fluorescein-disodium salt (Acros Organics B.V.B.A., Thermofisher Scientific, the Netherlands) and 500 ml of 1.8 g/l of NaCl (J.T. Baker, the Netherlands) solution in Inj_1 and Inj_2, sequentially in order to avoid any influence of fluorescein-disodium salt on the electric conductivity, and therefore interference with the NaCl breakthrough curves. Because of the uniqueness of the DNA sequences in the SiDNAmags, we injected the different particles at the same time. The fluorescein and NaCl concentrations were analysed by measuring the absorbance at 489 nm using UV–visible spectrometer (Lambda 365, PerkinElmer, USA) and electric conductivity (Cond3310, WTW, Wiilheim, Germany), respectively. SiDNAmag concentrations were quantified by measuring DNA concentrations using quantitative polymerase chain reaction (qPCR) (Biorad, USA), as described by Chakraborty et al. (2022). The salt tracer breakthrough datapoints (Fig. 3), were background concentration subtracted as

$$\frac{EC}{EC_0} = \frac{EC - EC_{BG}}{EC_0 - EC_{BG}} \quad (2)$$

where EC, EC_0, and EC_{BG} [μS/cm], were observed, injected and background electric conductivity. We presented the salt and SiDNAmag breakthrough curves with only the datapoints above the background concentration and No template control (NTC), respectively.

2.3. Breakthrough curve analysis and 3D modelling

We compared the characteristics of the experimental breakthrough curves (BTC) between the salt tracers and SiDNAmags in terms of time of maximum effluent concentration (t_{peak}), maximum effluent relative concentration (C_{max}/C_0) and time of C_{max}/C_0 for all sampling locations. Then we estimated the distributions of the α_L, α_{TV}/α_L, and α_{TH}/α_L of the salt tracers and the SiDNAmags, by subjecting the BTCs to convective-diffusive transport modelling adopting a Monte Carlo approach.

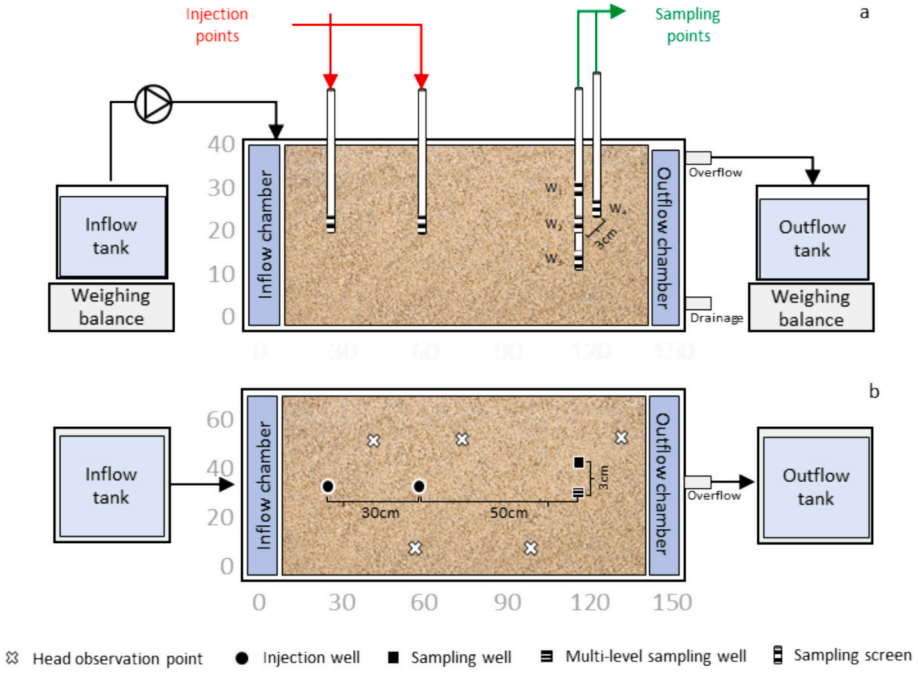

Fig. 2. Schematic experimental setup.

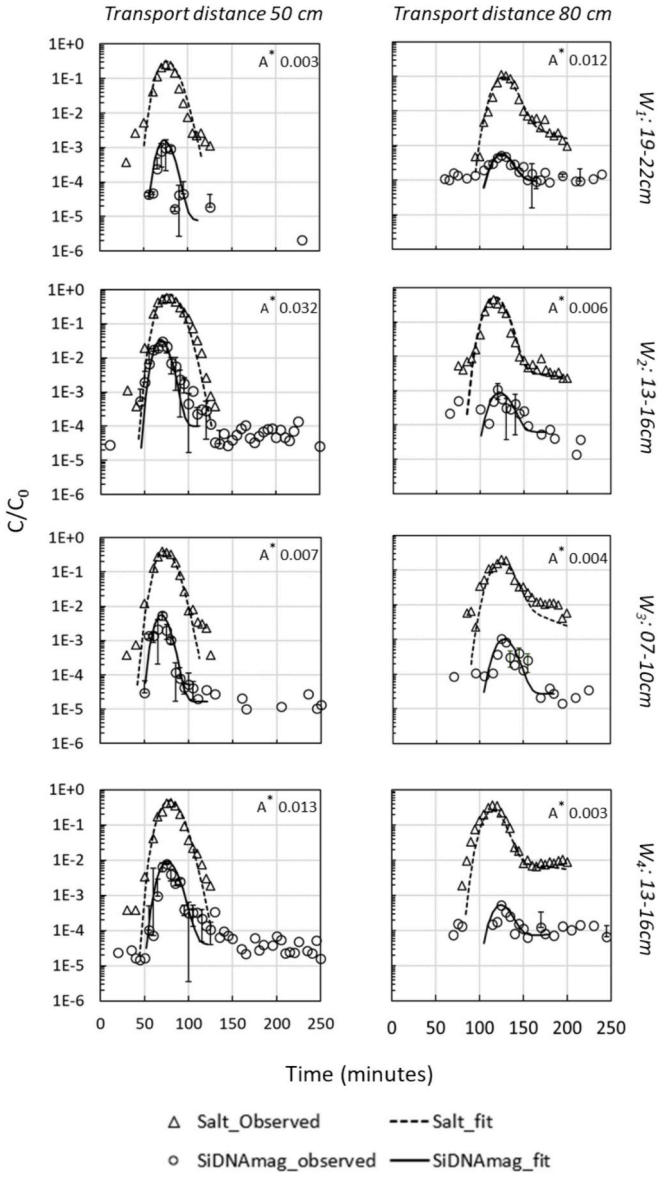

Fig. 3. Breakthrough curves of conservative (NaCl, fluorescein) and SiDNAmag for 50 cm (1a, 2a, 3a and 4a) and 80 cm (1b, 2b, 3b, 4b) transport distance at W_1, W_2, W_3 and W_4 sampling locations.

2.4. Monte Carlo simulation and parameter uncertainty analysis

We estimated the α_L, α_{TV}/α_L, and α_{TH}/α_L distributions using a 3D block-centred finite difference groundwater flow model Modflow-2005 (Harbaugh et al., 2017) in combination with the mass transport module, MT3DMS (Zheng and Wang, 1999). We solved the groundwater flow (equation not shown) in conjunction with solute transport (eq. 3) equation using an iteration based generalized conjugate solver in a python package, FloPy (Bakker et al., 2016). For the simulations, we used only the observed datapoints above background concentration (for NaCl and fluorescein) and above no template control (for SiDNAmags). Thereto, we could negate the influence of the datapoints below the background concentrations on the objective function. We considered first order kinetic attachment and detachment processes were the differences between the salt tracer and the SiDNAmag transport through the saturated sand (Chakraborty et al., 2022). The mass (salt and SiDNAmag) transport equation (Zheng and Wang, 1999) was

$$n_e\frac{\partial C}{\partial t}+k_{att}n_eC-k_{det}\rho_bS=\frac{\partial}{\partial x_i}\left(n_eD_{ij}\frac{\partial C}{\partial x_j}\right)-\frac{\partial}{\partial x_i}(n_ev_iC) \quad (3)$$

Where n_e is the effective porosity of the sand [−], C is the concentration of the salt tracer or SiDNAmag in the water, D_{ij} is the hydrodynamic dispersion coefficient tensor [m^2/min], k_{att} and k_{det} are the first order kinetic attachment and detachment rates of the colloids [1/min], v_i is the linear pore water velocity [m/min], S is the SiDNAmag concentration at the solid surface of the sand [kg/kg], ρ_b is the bulk density of the sand [kg/m^3] and t is the time [min]. In the mass transport module for SiDNAmag transport, k_{att} is expressed as β/n_e [1/min] and k_{det} is expressed as $\beta/\rho_b k_d$ [1/min], where β is the mass transfer rate from water to sand [1/min] and k_d is the distribution coefficient [m^3/kg] (Babakhani, 2019). We did not consider straining to be important since the colloid to sand grain diameter ratio was well below the threshold of 0.004 (Johnson et al., 2010) or 0.003 (Bradford and Bettahar, 2006). Though fluorescein dye is conventionally used as non-reactive conservative tracer, a number of studies had demonstrated a weak sorption capacity of fluorescein onto soils (Gerke et al., 2008; Torrentó et al., 2018). Therefore, we included the attachment and detachment terms for fluorescein as well.

We discretized the 0.36 m high sand tank spatially in 12 horizontal and variably confined-unconfined layers of equal thickness considering a specified constant head boundary condition. We temporally discretized transient mass transport simulations with a Dirichlet boundary condition in three stress periods (50, 1, 300 min) for stabilizing the hydraulic head distribution, solute or SiDNAmag injection and sampling period, respectively. We estimated the input ranges of hydraulic conductivity (K) from the Darcy flux and observed hydraulic gradients in observation wells. In a homogeneous groundwater flow model, (MODFLOW-2005 in a python package, FloPy), we also solved groundwater flow equation, for 10,000 random-uniformly sampled parameter value sets (Monte Carlo realizations) of K and n_e to simulate the observed hydraulic heads and optimize K and n_e. Based on the maximum objective function (coefficient of determination, R (Babakhani, 2019), we considered the best 1% of the K and n_e value sets as the input ranges. The input ranges of K and n_e were 0.07–0.1 m/min and 0.2–0.4 [−], respectively. In the homogeneous flow model, combined with a 3D mass transport module (MT3DMS), we solved the mass transport equation (eq. 3) for 10,000 random – uniformly sampled parameter sets (Monte Carlo realizations) of α_L, α_{TH}/α_L, and α_{TV}/α_L. The input ranges for α_L, α_{TV}/α_L, and α_{TH}/α_L were 10^{-6}–10^{-1} [m], 0.01–1, and 0.01–1, respectively for both the salt tracer and the SiDNAmag. For SiDNAmag transport simulations, we used input ranges of 0.001–0.1 [1/min] and 0.001–0.1 [m^3/kg], for β and k_d, respectively, to represent the first order kinetic attachment and detachment of SiDNAmag onto the collector sand grains. The goodness of fit of the parameter sets were evaluated based on root mean squared error (RMSE), both for individual sampling locations and combined for all sampling locations and transport distances (C-RMSE) (Ward et al., 2017). Based on the least C-RMSE, we considered the best 1% parameter sets as the parameter sets to construct the distributions of α_L, α_{TH}/α_L, and α_{TV}/α_L. We assessed the normality of the distributions using Kolmogorov – Smirnov test and Quantile – Quantile plot (QQ plot). Due to non-normality of few of the distributions, we evaluated the statistical significance of differences for each parameter, for conservative tracers and SiDNAmag using distribution non-specific Mann Whitney U test. The fitted breakthrough curves (Fig. 3) were based on the best parameter sets obtained for each parameter.

3. Results

3.1. SiDNAmag and sand characterization

The ζ potential of the two SiDNAmags (at a concentration of ~10^7

particles/ml) were − 22.9 ± 0.05 and − 22.06 ± 4.3 mV in the tap water, respectively. The D_{hyd} for the SiDNAmags were 586 ± 30.7 and 688 ± 69.5 nm, respectively. Under quiescent condition, D_{hyd} of the SiDNAmags, did not alter significantly throughout the experiment interval (Table 2), indicating SiDNAmag aggregation was unlikely to occur during the experiments. The ζ potential of the quartz sand was −26.3 ± 7.9 mV, suggesting an unfavourable SiDNAmag – sand grain attachment condition.

3.2. Conservative and SiDNAmag breakthrough curves

The t_{peaks} of the salt tracer for 0.5 m transport distance ranged between 70 and 80 min, similar to 70–75 min for SiDNAmag. At 0.8 m transport distance the t_{peaks} of the salt tracer ranged between 115 and 125 min, which was similar to the t_{peaks} of 120–125 min for the SiDNAmag (Table 2). For both the salt tracer and SiDNAmag, we observed maximum effluent concentration at W_2, as compared to W_1, W_3 and W_4, due to sampling at the same depth (0.13–0.16 m from the bottom of the tank) and flow line as the injection depth. A $C_{max}/C_0 < 1$ for salt tracer was due to mixing through longitudinal dispersion, horizontal transverse and vertical transverse dispersion. We observed a 1–3 log reduction in C_{max}/C_0 of SiDNAmag as compared to the salt tracer, and SiDNAmag to salt mass recovery ratio of 0.003–0.032, due to first order kinetic attachment in combination with α_L, α_{TH}, α_{TV}, and SiDNAmag plume mixing with background water (Fig. 3). Except for the sampling location W_1 for 0.5 m transport distance, all breakthrough curves had breakthrough curve tailing. The tailings were possibly due to the detachment of the SiDNAmags from sand grains. However, we did not include the complete tail datapoints in the modelling and parameter estimation process since the SiDNAmag concentrations were near no template control (NTC) and similar to the scattered datapoints prior to the breakthrough. Therefore, we treated the breakthrough tail datapoints near NTC as sample analysis uncertainty and did not include for the parameter estimation method. For fluorescein, injected at a transport distance of 0.8 m from the sampling points, we observed breakthrough tailing, possibly due to the detachment of the attached fluorescein from the sand grains (Table 2).

3.3. Parameter estimation

The RMSE of the individual sampling locations for 50 cm transport distance ranged between 0.034 and 0.074 and 0.006–0.085 for the salt and SiDNAmag, respectively. For 80 cm transport distance, the RMSE of the individual sampling locations ranged between 0.029 and 0.105 and 7.93×10^{-5}–2.22×10^{-4} for salt and SiDNAmag, respectively. C-RMSE for both the transport distances and all sampling locations ranged between 0.023 and 0.025 and 1.86×10^{-3} - 1.97×10^{-3} for the salt tracer and the SiDNAmag. Based on the best 1% parameter sets estimated from objective function of RMSE for all sampling points combined, the median K values for the salt and the SiDNAmag were 0.078 and 0.082 m/min, respectively. The K value uncertainty (5th – 95th percentile) for the salt tracer and the SiDNAmag were 0.074–0.081, and 0.079–0.085 m/min, respectively. Parameter distributions of n_e for all the sampling locations combined ranged between 0.29 and 0.35, and 0.27–0.35 [−], for the salt and SiDNAmag, respectively.

The median α_L, for the salt and the SiDNAmag estimated from sampling locations combined were 4.9×10^{-4} and 5.8×10^{-4} m, with a 5th – 95th percentile ranges of 6.7×10^{-5}–9.1×10^{-4}, and 5.6×10^{-5}–9.5×10^{-4} m, respectively. The median α_{TH}/α_L, and the α_{TV}/α_L for both the salt and the SiDNAmag estimated from all sampling points combined ranged between 0.52 and 0.56 [−] with a 5th – 95th percentile of 0.09–0.94 [−]. The 5th – 95th percentile ranges for each parameter for combined simulations are summarized in Table 2. A QQ plot and Kolmogorov – Smirnov test analysis (data not shown) indicated non-normality of the parameter distributions of the α_L, α_{TH}/α_L, and α_{TV}/α_L. The distributions of all the three parameters estimated either from individual sampling location or from all locations combined for SiDNAmag were not statistically significantly different from the parameter distributions estimated from salt tracer breakthrough curves, when compared using distribution non-specific Mann Whitney *U* test. The parameter distributions of k, n_e, α_L, α_{TV}/α_L, and α_{TH}/α_L, estimated from the salt and SiDNAmag breakthrough curves, and simulations combined for all transport distances and sampling locations has been shown as box plots with 5th – 95th percentile ranges in Fig. 4. For both the salt and the SiDNAmag, the parameter values and uncertainty ranges estimated from individual sampling locations were statistically similar to the all sampling locations combined. Therefore, we presented only the ranges estimated from all sampling locations combined.

The 1–3 log reduction in the C_{max}/C_0 of SiDNAmag, as compared to the conservative salt tracer was due to first order kinetic attachment of SiDNAmag onto the collector grains. The k_{att} for simulations combined for all the sampling locations and distances was 0.063 [1/min] with a 5th – 95th percentile ranges of 0.055–0.11 [1/min]. The k_{det} of the combined simulations was 3.26×10^{-4} [1/min] with a 5th – 95th percentile range of 1.48×10^{-4} to 1.58×10^{-3} [1/min]. The k_{det} were approximately 3 orders of magnitude lesser than that of k_{att}. The tailing of the fluorescein breakthrough curves could be explained through a low first order kinetic sorption ranging between 8.5×10^{-4} - 1.9×10^{-4} [1/min], indicating the weak sorption behaviour of fluorescein.

4. Discussion

The statistically similar α_L, α_{TH}/α_L, and α_{TV}/α_L parameter distributions for both the salt tracer and the SiDNAmag indicated that SiDNAmags had similar 3D dispersive behaviour as the salt tracer. The 1–3 log difference in maximum effluent concentration between the salt tracer and the SiDNAmags implied that a significant fraction of injected SiDNAmags could reach the sand grain surfaces, which are the low velocity regions in the parabolic Poiseuille's velocity profile in pores and pore throats, leading to colloid attachment onto the collector grains. Further, as observed by Auset and Keller (2004) in micromodel for smaller colloids (2 μm), the SiDNAmags possibly tended to remain in the low velocity streamlines and migrated along the sand grain surfaces. Therefore, SiDNAmags were not restricted to high velocity streamlines. Hence, as observed by Auset and Keller (2004) and Guo et al. (2016) for smaller particles in microscale, in our experiments the SiDNAmags probably travelled through as tortuous path as the salt tracer, resulting in similar 3D dispersive behaviour. In addition to low diffusion, the sand – SiDNAmag repulsion (charge exclusion) probably was not significant enough to force the SiDNAmags to move from grain surface (low velocity streamlines) towards the high velocity streamlines (Puls and Powell, 1992).

The SiDNAmags did not exhibit an earlier breakthrough or velocity enhancement at any of the sampling locations. This could be due to two orders of magnitude higher pore throat size as compared to the SiDNAmag diameter. This ratio was higher than the threshold of d_t/d_c of 1.5, the ratio below which colloids cannot enter the pore (Sirivithayapakorn and Keller, 2003). However, our results were not similar to Mikutis et al. (2018), even with similar colloid size (159 nm) and sand grain size (200 - 630 μm) used in both the studies. Unlike Mikutis et al. (2018), we did not observe increased colloid velocity and increased longitudinal dispersivity. The difference could be due to lower Darcy (0.2 cm/min) and average linear velocity (0.65 cm/min) applied in our sand tank, as longitudinal dispersivity of colloids was reported to increase with increasing interstitial fluid velocity, by Chrysikopoulos and Katzourakis (2015).

At the lowest average linear velocity (0.5 cm/min), which was similar to our study (~0.65 cm/min), Chrysikopoulos and Katzourakis (2015) did not observe velocity enhancement for any of the colloid sizes. However, the longitudinal dispersivity of colloids was higher than the conservative tracer, which could be due to the larger glass beads (2000 μm) than the mean sand grain diameter we used (630 μm). This is

Table 2
Salt and SiDNAmag breakthrough curves characteristics and estimated parameter distributions for hydraulic conductivity, effective porosity, longitudinal dispersivity, vertical and horizontal transverse dispersivities. The parameter ranges are presented as median (5th – 95th percentile) (K_{att} and K_{det} was not considered for 0.5 transport length since we assumed no sorption-desorption for NaCl tracer).

	Transport distance [m]		Tracer characteristics					BTC characteristics		Parameter distributions						
			ζ - potential [mV]	D_{hyd} [nm]				C_{max}/C_0 [−]	t_{peak} [min]	K [m/min]	n_e [−]	α_L [m]	α_{TH}/α_L [−]	α_{TV}/α_L [−]	K_{att} [1/min]	K_{det} [1/min]
				0 min	60 min	120 min	240 min									
Salt tracer	0.5	W_1	–	–				2.5×10^{-1}	75	0.078 (0.074–0.081)	0.31 (0.29–0.35)	4.9×10^{-4} (6.7×10^{-5} - 9.1×10^{-4})	0.55 (0.12 - 0.92)	0.56 (0.1 - 0.94)	–	–
		W_2						5.7×10^{-1}	75							
		W_3						5.0×10^{-1}	70							
		W_4						4.2×10^{-1}	80							
	0.8	W_1						1.1×10^{-1}	120						8.5×10^{-4} –1.9 $\times 10^{-3}$	5×10^{-7}–1.1 $\times 10^{-6}$
		W_2						4.4×10^{-1}	115							
		W_3						3.9×10^{-1}	115							
		W_4						1.9×10^{-1}	125							
SiDNAmag	0.5	W_1	22.9 ± 0.05	586 ± 31	547 ± 41	525 ± 81	599 ± 99	9.5×10^{-4}	70	0.082 (0.079 - 0.085)	0.31 (0.27 0.35)	5.8×10^{-4} (5.6×10^{-5} - 9.5×10^{-4})	0.52 (0.09 - 0.94)	0.56 (0.09 - 0.92)	0.063 (0.05–0.1)	3.2×10^{-4} (1.5×10^{-4} - 1.6×10^{-3})
		W_2						2.9×10^{-2}	70							
		W_3						5.3×10^{-3}	70							
		W_4						7.7×10^{-3}	75							
	0.8	W_1	22.06 ± 4.3	688 ± 69	625 ± 52	613 ± 89	688 ± 79	5.1×10^{-4}	125							
		W_2						1.1×10^{-2}	120							
		W_3						5.3×10^{-4}	120							
		W_4						1.0×10^{-4}	125							

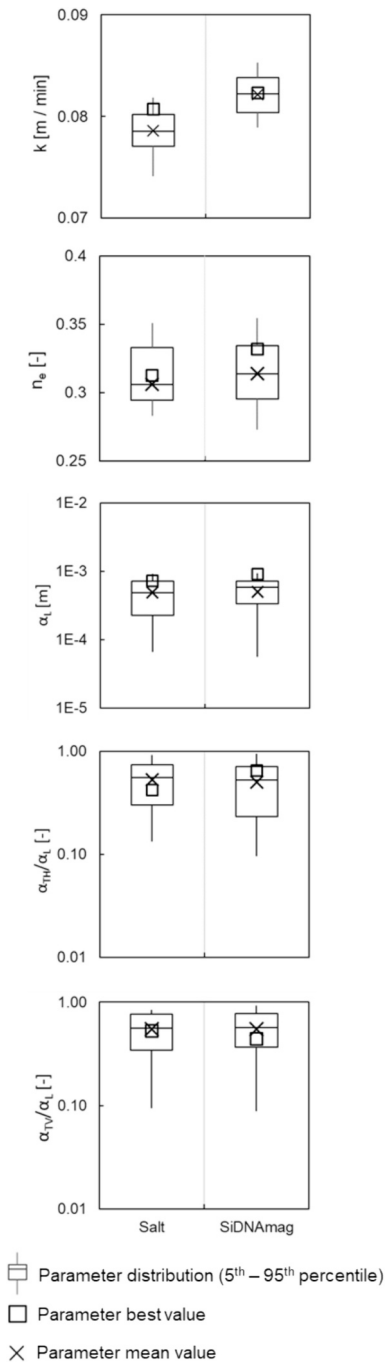

Fig. 4. Parameter distribution of α_L [m] (a), α_{TH} /α_L [−] (b) and α_{TV} /α_L [−] (c), for conservative tracers (NaCl and Fluorescein) and SiDNAmag particles. (Box = quartiles; horizontal line = median; whiskers = 5th – 95th percentile; X = mean of the distribution.

because smaller grain size produces less heterogeneity in the pore size distribution and more irregularity in grain shape increases continuity between medium and large pores (He et al., 2021). Heterogeneity in pore size distribution, in turn, influences the longitudinal dispersivity of colloids (Baumann et al., 2010). In addition, a linear increase in longitudinal dispersivity of colloids as compared to conservative tracer was also observed with increasing interstitial velocity (Chrysikopoulos and Katzourakis, 2015). In our work, the average linear velocity of pore water, therefore, was possibly sufficiently low to observe statistically similar longitudinal dispersivity of SiDNAmag, as compared to salt tracers. While using a 25 nm diameter silica particle, which was approximately 9–10 times smaller than our SiDNAmag, the earlier breakthrough of silica particles, as compared to conservative tritium tracer, observed by Higgo et al. (1993) in column experiments, was possibly due to the wide grain size distribution of the column sand (0.5–1000 μm) and therefore heterogeneity in the pore size distribution. This possibly explains why our results differ with regards to the occurrence of size exclusion observed in saturated sand columns by Higgo et al. (1993). It was not possible to reconcile the results of this study with the observations of varying extent of size exclusion, velocity enhancement and longitudinal dispersivity alteration for colloids reported by Grolimund et al. (1998); Higgo et al. (1993); James and Chrysikopoulos (2003); Keller et al. (2004) due to the differences in all the experimental conditions, such as, flow rate, average linear velocity, colloid size and porous media grain size.

In our study, the ratio of median transverse dispersivities for both the salt tracer and the SiDNAmag was higher than the oftentimes accepted value of 0.1 (Bijeljic and Blunt, 2007). This is possibly due to a low peclet number and a low average fluid velocity. Bijeljic and Blunt (2007) reported the α_{TV} /α_L and α_{TH} /α_L for solutes can be as high as ~1 at low peclet number (0.5–1) and decreased with increasing peclet number. In order to further characterize the mechanism of 3D dispersion of SiDNAmags and compare with the salt tracer, a pore scale modelling is required (Auset and Keller, 2004; Baumann et al., 2010). However, pore scale observation was not within the scope of this study.

While our research underscored the usefulness of SiDNAmag in determining the longitudinal and transverse dispersivities of sand media, it is essential to acknowledge the limitations of this study. The universality of our finding that the longitudinal dispersivity, transverse dispersivity and associated uncertainties estimated form the salt tracer and SiDNAmag were statistically not different, is restricted. This is because the colloid transport and dispersivities in porous media, in general, is dependent on several physico-chemical experimental conditions. Dispersivities of colloidal particles depend on sand grain size (Syngouna and Chrysikopoulos, 2011), colloid diameter (Auset and Keller, 2004; Guo et al., 2016), and flow velocity (Auset and Keller, 2004). Our conclusion that dispersivities of SiDNAmag was similar to those of salt tracers apply sand grain size and colloid diameter used in this study. Transport behaviour of SiDNAmag was analysed from fitting a first order kinetic attachment – detachment model to the breakthrough curves. This approach did not allow to distinguish between colloid retention mechanisms.

5. Conclusion

5.1. From the salt tracer and colloid (SiDNAmag) particle transport experiments, under our experimental conditions, we found that the longitudinal dispersivity, horizontal transverse and vertical transverse dispersivities of SiDNAmags were similar to the salt tracers. Therefore, we can accept our null hypothesis.

5.2. The parameter distributions of longitudinal dispersivity, horizontal and vertical transverse dispersivities estimated from the individual sampling locations were not statistically significantly different as compared to the distributions estimated from the simulations combined for all sampling distance and locations.

5.3. The SiDNAmags did not show size exclusion or velocity enhancement under current experimental conditions. Due to that, the longitudinal and transverse dispersivities for SiDNAmags were similar to the salt tracer.

5.4. The implication of this study lies in, as applied in our experiments, when the collector grain diameter is few orders of magnitude higher than the colloid diameter, the colloids have similar three-dimensional dispersive behaviour and can be applied to predict the transport of solute tracer plumes in 3D.

5.5. However, SiDNAmag attachment onto the collector sand grains reduced the maximum effluent concentration by 1–3 orders of magnitude as compared to the conservative salt tracer, indicating a potential

limitation of SiDNAmag application in investigations involving long transport distances.

CRediT authorship contribution statement

Swagatam Chakraborty: Writing – review & editing, Writing – original draft, Visualization, Methodology, Data curation, Conceptualization. **Rayan Elhaj:** Investigation. **Jan Willem Foppen:** Writing – review & editing, Supervision, Resources, Methodology, Investigation, Conceptualization. **Jack F. Schijven:** Writing – review & editing, Supervision, Resources, Methodology, Conceptualization.

Declaration of competing interest

The authors declare that they have no known competing financial interests or personal relationships that could have appeared to influence the work reported in this paper.

Data availability

The data can be available upon request.

Acknowledgement

This research had been funded by the Dutch Research Council (NWO), TTW grant 14514. We would like to thank Dr. Sulalit Bandyopadhyay, Department of Chemical Engineering, Faculty of Natural Sciences, NTNU, Norway for the kind contribution with SiDNAmag particles. We would like extend our gratitude to thank Dr. Thom Bogaard, Department of Civil Engineering and Geosciences, TU-Delft, the Netherlands, for his contribution and support with experimental setup preparation and modelling. We would like to thank Hortus Botanicus, TU-Delft, the Netherlands; and IHE-Delft, the Netherlands for the laboratory work support. We would also like to thank Mr. Fuad Alqrinawi for his technical contribution in developing the code for Monte Carlo simulation.

References

Auset, M., Keller, A., 2004. Pore-scale processes that control dispersion of colloids in saturated porous media. Water Resour. Res. 40 (3) https://doi.org/10.1029/2003WR002800.

Babakhani, P., 2019. The impact of nanoparticle aggregation on their size exclusion during transport in porous media: one-and three-dimensional modelling investigations. Sci. Rep. 9 (1), 1–12. https://doi.org/10.1038/s41598-019-50493-6.

Bakker, M., Post, V., Langevin, C.D., Hughes, J.D., White, J.T., Starn, J.J., Fienen, M.N., 2016. Scripting MODFLOW model development using Python and FloPy. Groundwater 54 (5), 733–739. https://doi.org/10.1111/gwat.12413.

Baumann, T., Toops, L., Niessner, R., 2010. Colloid dispersion on the pore scale. Water Res. 44 (4), 1246–1254. https://doi.org/10.1016/j.watres.2009.11.035.

Bennacer, L., Ahfir, N.D., Bouanani, A., Alem, A., Wang, H., 2013. Suspended particles transport and deposition in saturated granular porous medium: particle size effects. Transp. Porous Media 100 (3), 377–392. https://doi.org/10.1007/s11242-013-0220-4.

Bijeljic, B., Blunt, M.J., 2007. Pore-scale modeling of transverse dispersion in porous media. Water Resour. Res. 43 (12) https://doi.org/10.1029/2006WR005700.

Bradford, S.A., Bettahar, M., 2006. Concentration dependent transport of colloids in saturated porous media. J. Contam. Hydrol. 82 (1–2), 99–117. https://doi.org/10.1016/j.jconhyd.2005.09.006.

Chakraborty, S., Foppen, J.W., Schijven, J.F., 2022. Effect of concentration of silica encapsulated ds-DNA colloidal microparticles on their transport through saturated porous media. Colloids Surf. A Physicochem. Eng. Asp. 651, 129625 https://doi.org/10.1016/j.colsurfa.2022.129625.

Chakraborty, S., Elhaj, R., Foppen, J.W., Schijven, J., 2023. Effect of injection water ionic strength on estimating hydraulic parameters in a 3D sand tank using silica encapsulated magnetic DNA particles. Adv. Water Resour. 104507 https://doi.org/10.1016/j.advwatres.2023.104507.

Chrysikopoulos, C.V., Katzourakis, V.E., 2015. Colloid particle size-dependent dispersivity. Water Resour. Res. 51 (6), 4668–4683. https://doi.org/10.1002/2014WR016094.

Chrysikopoulos, C.V., Syngouna, V.I., 2014. Effect of gravity on colloid transport through water-saturated columns packed with glass beads: modeling and experiments. Environ. Sci. Technol. 48 (12), 6805–6813. https://doi.org/10.1021/es501295n.

Dahlke, H.E., Williamson, A.G., Georgakakos, C., Leung, S., Sharma, A.N., Lyon, S.W., Walter, M.T., 2015. Using concurrent DNA tracer injections to infer glacial flow pathways. Hydrol. Process. 29 (25), 5257–5274. https://doi.org/10.1002/hyp.10679.

de Vries, E.T., Tang, Q., Faez, S., Raoof, A., 2022. Fluid flow and colloid transport experiment in single-porosity sample; tracking of colloid transport behavior in a saturated micromodel. Adv. Water Resour. 159, 104086 https://doi.org/10.1016/j.advwatres.2021.104086.

Foppen, J.W., 2023. Artificial DNA in hydrology. Wiley interdisciplinary reviews. Water e1681. https://doi.org/10.1002/wat2.1681.

Foppen, J.W., Orup, C., Adell, R., Poulalion, V., Uhlenbrook, S., 2011. Using multiple artificial DNA tracers in hydrology. Hydrol. Process. 25 (19), 3101–3106. https://doi.org/10.1002/hyp.8159.

Gerke, K.M., Sidle, R.C., Tokuda, Y., 2008. Sorption of Uranine on forest soils. Hydrological Research Letters 2, 32–35. https://doi.org/10.3178/hrl.2.32.

Grolimund, D., Elimelech, M., Borkovec, M., Barmettler, K., Kretzschmar, R., Sticher, H., 1998. Transport of in situ mobilized colloidal particles in packed soil columns. Environ. Sci. Technol. 32 (22), 3562–3569. https://doi.org/10.1021/es980356z.

Guo, Y., Huang, J., Xiao, F., Yin, X., Chun, J., Um, W., Wu, N., 2016. Bead-based microfluidic sediment analogues: fabrication and colloid transport. Langmuir 32 (36), 9342–9350. https://pubs.acs.org/doi/abs/10.1021/acs.langmuir.6b02184.

Harbaugh, A.W., Langevin, C.D., Hughes, J.D., Niswonger, R.N., Konikow, L.F., 2017. MODFLOW-2005 version 1.12. 00, the US geological survey modular groundwater model. US Geological Survey Software Release 3.

He, S.H., Ding, Z., Hu, H.B., Gao, M., 2021. Effect of grain size on microscopic pore structure and fractal characteristics of carbonate-based sand and silicate-based sand. Fractal and Fractional 5 (4), 152. https://doi.org/10.3390/fractalfract5040152.

Higgo, J.J.W., Williams, G.M., Harrison, I., Warwick, P., Gardiner, M.P., Longworth, G., 1993. Colloid transport in a glacial sand aquifer. Laboratory and field studies. In: Colloids in the Aquatic Environment. Elsevier, pp. 179–200. https://doi.org/10.1016/B978-1-85861-038-2.50016-4.

James, S.C., Chrysikopoulos, C.V., 2003. Effective velocity and effective dispersion coefficient for finite-sized particles flowing in a uniform fracture. J. Colloid Interface Sci. 263 (1), 288–295. https://doi.org/10.1016/S0021-9797(03)00254-6.

Johnson, W.P., Pazmino, E., Ma, H., 2010. Direct observations of colloid retention in granular media in the presence of energy barriers, and implications for inferred mechanisms from indirect observations. Water Res. 44 (4), 1158–1169. https://doi.org/10.1016/j.watres.2009.12.014.

Katzourakis, V.E., Chrysikopoulos, C.V., 2021. Modeling the transport of aggregating nanoparticles in porous media. Water Resour. Res. 57 (1), e2020WR027946 https://doi.org/10.1029/2020WR027946.

Keller, A.A., Sirivithayapakorn, S., Chrysikopoulos, C.V., 2004. Early breakthrough of colloids and bacteriophage MS2 in a water-saturated sand column. Water Resour. Res. 40 (8) https://doi.org/10.1029/2003WR002676.

McCarthy, J.F., 2018. Sampling and characterization of colloids and particles in groundwater for studying their role in contaminant transport. In: Environmental particles. CRC Press, pp. 247–315.

Meng, X., Yang, D., 2019. Pore-network modeling of particle dispersion in porous media. Colloids Surf. A Physicochem. Eng. Asp. 580, 123768 https://doi.org/10.1016/j.colsurfa.2019.123768.

Mikutis, G., Deuber, C.A., Schmid, L., Kittilä, A., Lobsiger, N., Puddu, M., Stark, W.J., 2018. Silica-encapsulated DNA-based tracers for aquifer characterization. Environ. Sci. Technol. 52 (21), 12142–12152. https://doi.org/10.1021/acs.est.8b03285.

Pang, L., Abeysekera, G., Hanning, K., Premaratne, A., Robson, B., Abraham, P., Billington, C., 2020. Water tracking in surface water, groundwater and soils using free and alginate-chitosan encapsulated synthetic DNA tracers. Water Res. 184, 116192 https://doi.org/10.1016/j.watres.2020.116192.

Pang, L., Lin, S., Hewitt, J., Premaratne, A., Close, M., 2021. Attenuation and transport of human enteric viruses and bacteriophage MS2 in alluvial sand and gravel aquifer media—laboratory studies. Water Res. 196, 117051 https://doi.org/10.1016/j.watres.2021.117051.

Puls, R.W., Powell, R.M., 1992. Transport of inorganic colloids through natural aquifer material: implications for contaminant transport. Environ. Sci. Technol. 26 (3), 614–621. https://doi.org/10.1021/es00027a027.

Ren, X.W., Santamarina, J.C., 2018. The hydraulic conductivity of sediments: a pore size perspective. Eng. Geol. 233, 48–54. https://doi.org/10.1016/j.enggeo.2017.11.022.

Schijven, J.F., van den Berg, H.H., Colin, M., Dullemont, Y., Hijnen, W.A., Magic-Knezev, A., Wubbels, G., 2013. A mathematical model for removal of human pathogenic viruses and bacteria by slow sand filtration under variable operational conditions. Water Res. 47 (7), 2592–2602. https://doi.org/10.1016/j.watres.2013.02.027.

Sharma, A.N., Luo, D., Walter, M.T., 2012. Hydrological tracers using nanobiotechnology: proof of concept. Environ. Sci. Technol. 46 (16), 8928–8936. https://doi.org/10.1021/es301561q.

Sharma, A., Foppen, J.W., Banerjee, A., Sawssen, S., Bachhar, N., Peddis, D., Bandyopadhyay, S., 2021. Magnetic nanoparticles to unique DNA tracers: effect of functionalization on Physico-chemical properties. Nanoscale Res. Lett. 16 (1), 1–16. https://doi.org/10.1186/s11671-021-03483-5.

Sirivithayapakorn, S., Keller, A., 2003. Transport of colloids in saturated porous media: a pore-scale observation of the size exclusion effect and colloid acceleration. Water Resour. Res. 39 (4) https://doi.org/10.1029/2002WR001583.

Solovitch, N., Labille, J., Rose, J., Chaurand, P., Borschneck, D., Wiesner, M.R., Bottero, J.Y., 2010. Concurrent aggregation and deposition of TiO2 nanoparticles in a sandy porous media. Environ. Sci. Technol. 44 (13), 4897–4902. https://doi.org/10.1021/es1000819.

Syngouna, V. I., & Chrysikopoulos, C. V. (2011). Transport of biocolloids in water saturated columns packed with sand: effect of grain size and pore water velocity. J. Contam. Hydrol., 126(3–4), 301–314. doi: https://doi.org/10.1016/j.jconhyd.2011.09.007.

Torrentó, C., Prasuhn, V., Spiess, E., Ponsin, V., Melsbach, A., Lihl, C., Hunkeler, D., 2018. Adsorbing vs. nonadsorbing tracers for assessing pesticide transport in arable soils. Vadose Zone J. 17 (1), 1–18. https://doi.org/10.2136/vzj2017.01.0033.

Tosco, T., Bosch, J., Meckenstock, R.U., Sethi, R., 2012. Transport of ferrihydrite nanoparticles in saturated porous media: role of ionic strength and flow rate. Environ. Sci. Technol. 46 (7), 4008–4015. https://doi.org/10.1021/es202643c.

Vasiliadou, I.A., Chrysikopoulos, C.V., 2011. Cotransport of pseudomonas putida and kaolinite particles through water-saturated columns packed with glass beads. Water Resour. Res. 47 (2) https://doi.org/10.1029/2010WR009560.

Wang, C., Bobba, A.D., Attinti, R., Shen, C., Lazouskaya, V., Wang, L.P., Jin, Y., 2012. Retention and transport of silica nanoparticles in saturated porous media: effect of concentration and particle size. Environ. Sci. Technol. 46 (13), 7151–7158. https://doi.org/10.1021/es300314n.

Wang, Y., Bradford, S.A., Šimůnek, J., 2013. Transport and fate of microorganisms in soils with preferential flow under different solution chemistry conditions. Water Resour. Res. 49 (5), 2424–2436. https://doi.org/10.1002/wrcr.20174.

Ward, A.S., Kelleher, C.A., Mason, S.J., Wagener, T., McIntyre, N., McGlynn, B., Payn, R. A., 2017. A software tool to assess uncertainty in transient-storage model parameters using Monte Carlo simulations. Freshwater Science 36 (1), 195–217. https://doi.org/10.1086/690444.

Won, J., Wirth, X., Burns, S.E., 2019. An experimental study of cotransport of heavy metals with kaolinite colloids. J. Hazard. Mater. 373, 476–482. https://doi.org/10.1016/j.jhazmat.2019.03.110.

Zech, A., Attinger, S., Bellin, A., Cvetkovic, V., Dietrich, P., Fiori, A., Dagan, G., 2019. A critical analysis of transverse dispersivity field data. Groundwater 57 (4), 632–639. https://doi.org/10.1111/gwat.12838.

Zhang, Y., Hartung, M.B., Hawkins, A.J., Dekas, A.E., Li, K., Horne, R.N., 2021. DNA tracer transport through porous media—the effect of DNA length and adsorption. Water Resour. Res. 57 (2) https://doi.org/10.1029/2020WR028382, 2020WR028382.

Zheng, C., Wang, P.P., 1999. MT3DMS: a modular three-dimensional multispecies transport model for simulation of advection, dispersion, and chemical reactions of contaminants in groundwater systems; documentation and user's guide. http://hdl.handle.net/11681/4734.